Emergence of a higher energy structure in strong field ionization with inhomogeneous electric fields

L. Ortmann[1],* J. A. Pérez-Hernández[2],† M. F. Ciappina[3,4], J. Schötz[3], A. Chacón[5], G. Zeraouli[2], M. F. Kling[3,6], L. Roso[2], M. Lewenstein[5,8], and A. S. Landsman[1,7‡]

[1]*Max Planck Institute for the Physics of Complex Systems, Nöthnitzer Straße 38, D-01187 Dresden, Germany*

[2]*Centro de Láseres Pulsados (CLPU), Parque Científico, Villamayor, Salamanca, Spain*

[3]*Max-Planck Institut für Quantenoptik, Hans-Kopfermann-Str. 1, D-85748 Garching, Germany*

[4]*Institute of Physics of the ASCR, ELI-Beamlines, Na Slovance 2, 182 21 Prague, Czech Republic*

[5]*ICFO-Institut de Ciències Fotòniques, The Barcelona Institute of Science and Technology, 08860 Castelldefels (Barcelona), Spain*

[6]*Department für Physik, Ludwig-Maximilians-Universität München, Am Coulombwall 1, D-85748 Garching, Germany*

[7]*Department of Physics, Max Planck Postech, Pohang, Gyeongbuk 37673, Republic of Korea and*

[8]*ICREA-Institució Catalana de Recerca i Estudis Avançats, Lluis Companys 23, 08010 Barcelona, Spain*

(Dated: June 21, 2017)

Studies of strong field ionization have historically relied on the strong field approximation, which neglects all spatial dependence in the forces experienced by the electron after ionization. More recently, the small spatial inhomogeneity introduced by the long-range Coulomb potential has been linked to a number of important features in the photoelectron spectrum, such as Coulomb asymmetry, Coulomb focusing, and the low energy structure (LES). Here, we demonstrate using mid-infrared laser wavelength that a time-varying spatial dependence in the laser electric field, such as produced in the vicinity of a nano-structure, creates a prominent higher energy peak. This higher energy structure (HES) originates from direct electrons ionized near the peak of a single half-cycle of the laser pulse. The HES is separated from all other ionization events, with its location and width highly dependent on the strength of spatial inhomogeneity. Hence, the HES can be used as a sensitive tool for near-field characterization in the "intermediate regime", where electron's quiver amplitude is comparable to the field decay length. Moreover, the large accumulation of electrons with tuneable energy suggests a promising method for creating a localized source of electron pulses of attosecond duration using *tabletop laser* technology.

When the photon energy of light is many times smaller than the ionization potential of an atom, the ionization process is described by either tunnel or multi-photon ionization [1–4]. These two regimes are separated by the Keldysh parameter $\gamma = \sqrt{I_p/2U_p}$, where I_p is the ionization potential and U_p is the ponderomotive energy of an electron in a laser field [5]. For $\gamma \leq 1$, the ionization process is dominated by tunneling, whereby the electric field of the laser bends the binding potential of the atom forming a barrier through which the electron tunnels out and is subsequently accelerated by the strong laser field [6]. Tunnel ionization underlies the creation of attosecond pulses via the process of high harmonic generation (HHG) [6–9], as well as a variety of other important applications, including photoelectron holography [10, 11], tomographic imaging of molecular orbitals [12] and electron diffraction [13–15].

Wavelengths used in tunnel ionization experiments are typically in the infrared (IR) range and have more recently been extended into the mid-IR regime [16–19]. Under these conditions, the laser field is well-described by the dipole approximation, resulting in spatially homogeneous time-varying electric fields. The strong field approximation (SFA) [5, 20, 21], which neglects the remaining Coulomb force on the ionized electron, has been the dominant tool for investigating electron dynamics under these circumstances. However, the small spatial dependence introduced by the $1/r$ Coulomb potential has led to a number of interesting phenomena, such as Coulomb asymmetry [22, 23] and Coulomb focusing [23, 24]. Of particular note is a discovery using mid-IR pulses of the low energy structure (LES) [16]. This surprising finding stimulated a great amount of experimental [18, 25–28] and theoretical work [27–32], and highlighted the dramatic impact that even a small spatial inhomogeneity in force can have on electron dynamics after strong field ionization. Here, we show that a field inhomogeneity in the mid-IR laser pulse produced by a nearby nano-structure creates a prominent peak at higher energies, or a higher energy structure (HES).

There has been significant interest in strong field ionization phenomena in the vicinity of a nanostructure [33–46]. A key characteristic of nanostructures is significant near-field enhancement, resulting in a time-dependent spatial inhomogeneity in the presence of a laser pulse. This spatial inhomogeneity introduces another parameter (in addition to γ), given by $\delta = l_F/l_q$, where l_F is the decay length and $l_q = eF/m\omega^2$ is the electron quiver amplitude, respectively [40]. For $\delta \gg 1$, the electron sees essentially a homogeneous laser field, while for $\delta \ll 1$, it immediately leaves the vicinity of a nanostructure. Here, we focus on a less understood and more complex "inter-

mediate regime" of $\delta \sim 1$.

Prior theoretical work using infrared laser pulses [47–49] found a large enhancement in electron yield forming an extended high energy tail. This enhancement resulted in a substantial extension in the maximum cut-off energy, well above the usual $10U_p$ cut-off for rescattered electrons [50]. In this letter, we focus instead on a higher energy structure (HES) found near $2U_p$, and characterized by a prominent hump. We show that this hump is made up of direct electrons ionized within a narrow time-window of the laser pulse and that moreover its width and location is determined by the decay length, l_F, of the near-fields.

Our approach combines the solution of a three-dimensional time-dependent Schrödinger equation (3D-TDSE) with classical trajectory Monte Carlo (CTMC) simulations, which account for the initial wavepacket distribution after tunnel ionization. The electric field in the vicinity of a nanotip decays exponentially. For sufficiently short distances, compared to the decay length, the time-dependent electric field can be approximated as [51],

$$\mathbf{E}(z,t) = E_0(1+2\beta z)f(t)\cos(\omega t+\varphi)\hat{z} \qquad (1)$$

where $\hat{z}$ is the direction of laser polarization (note that decreasing z signifies movement away from the tip), E_0 is the amplitude of the electric field at the location of the parent atom, ϕ is the carrier-envelope phase (CEP) and β is given by the inverse $(1/e)$ decay length: $2\beta = 1/l_F$. The pulse envelope is given by: $f(t) = \cos^2\left(\frac{\omega t}{2N}\right)$, where N is a number of cycles in a pulse.

Note that we use mid-IR pulses of the same wavelength ($\lambda = 2$ microns) as previously used in [16] to measure the LES. Such lower frequencies, compared to the previously used 800 nm light [47–49], are particularly beneficial for plasmonically enhanced fields since they result in greater electron excursion, thereby allowing an electron to explore more of the near-field. This, in turn, means that it is possible to use larger nano-structures, which have a greater decay length, and therefore increase the gas volume available for ionization in the near-field.

To calculate the energy-resolved photoelectron spectra, $P(E)$, we solve the 3D-TDSE in the length gauge following the method in [49]

$$\frac{i\partial\Psi(\mathbf{r},t)}{\partial t} = H\Psi(\mathbf{r},t) = \left[-\frac{\nabla^2}{2} + V(r) + V_l(\mathbf{r},t)\right]\Psi(\mathbf{r},t) \qquad (2)$$

where $V(r)$ is the atomic potential and $V_l(\mathbf{r},t) = -\int^{\mathbf{r}} d\mathbf{r}' \cdot \mathbf{E}(\mathbf{r}',t)$ represents interaction with the laser field. All the simulations were done within a single active electron approximation, using the potentials given in [52] and starting from the ground-state wavefunction.

Figure 1 shows the ATI spectra for hydrogen, helium and argon atoms calculated using 3D-TDSE for two different decay lengths, $l_F = 8.3$ nm ($\beta = 0.003$) and $l_F = 12.5$ nm ($\beta = 0.002$), corresponding to $\delta = 2.43$ and 1.62, respectively. As expected, the electron yield from helium is significantly lower than from hydrogen and argon due to a higher ionization potential. For all atoms, the HES structure disappears in the absence of spatial inhomogeneity. Note that the electrons comprising the HES are relatively high in energy, beyond the classical cutoff of $2U_p$ observed for direct electrons in homogeneous fields [16].

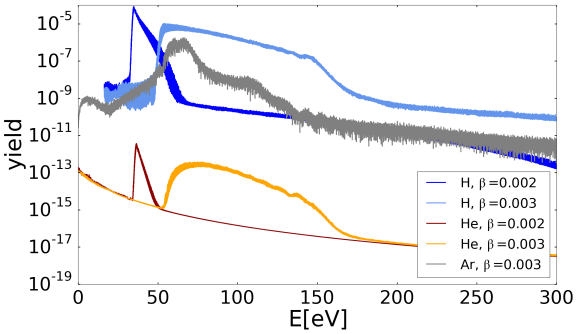

FIG. 1. 3D TDSE photoelectron spectra for hydrogen, helium and argon atoms generated by laser pulses described in Eq. (1) for different values of β parameters. The laser intensity at the atom is $I = 1\times10^{14}$W/cm^2 (or $E_0 = 0.0534$ a.u.), the wavelength $\lambda = 2000$ nm, the number of cycles $N = 2$ and CEP$= \pi$.

The prominent higher energy peak may at first glance look like a resonance. However, its location is independent of the atomic species and is determined instead by the decay length of the near-field. From CTMC simulations (see below for detail), we find that the location of the HES has a quadratic dependence on the field decay length:

$$E_{peak} \propto \left(\frac{1}{l_F}\right)^2 \qquad (3)$$

where E_{peak} is the kinetic energy of electrons comprising the peak of the HES. Analysis of the trajectories shows that these electrons are released at the center of the pulse envelope. This allows for an approximate analytical solution (see [53] for detail), whereby the scaling in Eqn. (3) can be derived by approximately integrating $a(t)$ from the electron's birth in the continuum until the end of the laser pulse t_{final} and finding that $v(t_{final})$ scales linearly with β and that therefore the final energy depends quadratically on $\beta = 1/(2l_F)$.

From Eqn. (3), increasing the spatial inhomogeneity will substantially accelerate the electrons. To understand the physical origin of the peak, we use CTMC simulations to investigate electron trajectories after ionization of hydrogen. Here, single trajectories are launched at a starting phase $\varphi_0 = \omega \cdot t_0$, with velocity $v_\perp$ perpendicular to the laser polarization direction. The probability distribution at the tunnel exit is given by the Ammosov Delone Krainov (ADK) formula [54, 55], typically used

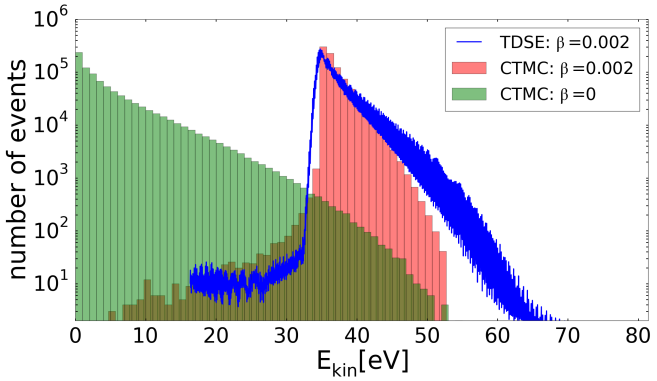

FIG. 2. Histogram of the photoelectron yield as a function of the final kinetic energy obtained in a CTMC calculation for hydrogen with the same laser parameters as given in Fig. 1 for two different values of β, where $\beta = 0$ corresponds to an homogeneous field. The blue line shows the same quantity as the red bars, but was obtained in a 3D TDSE calculation.

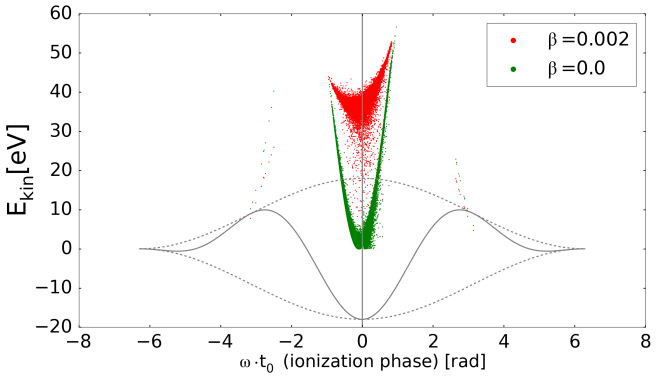

FIG. 3. Kinetic energy of photoelectrons as a function of ionization phase from a CTMC calculation for hydrogen for the same homogeneous ($\beta = 0$) and non-homogeneous ($\beta = 0.002$) electric fields as given in Fig. 1 and 2. Each dot corresponds to a single trajectory.

to model strong field ionization [56–59]:

$$P(t_0, v_\perp) = \exp\left(-\frac{2(2I_p)^{3/2}}{3E(t_0)}\right) \cdot \exp\left(-\frac{v_\perp^2\sqrt{2I_p}}{E(t_0)}\right), \quad (4)$$

where the laser field $E(t_0)$ is given by Eq. (1) with $z = 0$, corresponding to an atom centered at the origin, and I_p is the ionization potential [60]. The tunnel exit radius is obtained using parabolic coordinates [60–64]. The dynamics of each electronic trajectory after ionization is solved numerically by integrating the Newton's equations following the method in [61, 65].

Figure 2 shows electron yield as a function of energy obtained with CTMC simulations. Note that only direct electrons are shown, as rescattering events were not included in our classical simulations. As can be seen, the prominent higher energy peak (starting around 40 eV) observed in 3D-TDSE (blue curve) is well-reproduced. The surprising accuracy of the adiabatic ADK approximation is due to the low-frequency of laser light, which results in the Keldysh adiabaticity parameter $\gamma = 0.573$ – well within the tunnel ionization regime. The figure also includes the energy distribution for direct electrons in the absence of field inhomogeneity. As can be seen, the field inhomogeneity significantly accelerates a large fraction of the electrons.

Figure 3 establishes the physical origin of the HES by comparing the final electron kinetic energy as a function of ionization time, t_0, for homogeneous and inhomogeneous fields. By far, the most dramatic influence of the spatial inhomogeneity occurs in the central cycle, corresponding to the maximum probability of ionization along the direction of increasing field. As Fig. 3 shows, field inhomogeneity causes electrons ionized near the laser field maximum to get accelerated to over 30 eV, whereas these same electrons have much smaller energies in homogeneous fields. In fact, the electrons ionized near the peak by homogeneous fields are known to have low final energies (see also Fig. 3), thereby contributing to Rydberg states [57] and the zero energy structure [19, 27]. This also suggests, in agreement with prior findings [66], a depletion of long trajectory contributions to high harmonic generation, since these trajectories are made up of electrons ionized shortly after the peak of the laser field.

Importantly, in addition to accelerating, the field inhomogeneity also significantly narrows the electron energy distribution, leading to a well-defined peak observed in CTMC and TDSE simulations. Finally, since all electrons in the HES come from a single half-cycle, they are distinctly separated in energy from all other ionization events, suggesting that inter-cycle interference should only be observed at lower and higher electron energies. (Inter-cycle interference was absent for all energies from TDSE simulations due to the shortness of the pulse).

Based on the above analysis, the appearance of a HES should coincide with a depletion of low energy electrons, which get accelerated by the field inhomogeneity. This depletion can be clearly observed in Fig. 4, which shows 3D-TDSE simulations of electron momenta distributions for hydrogen for homogeneous and non-homogeneous electric fields. The high-energy electrons with positive (negative) momentum along the z axis come from a narrow time-window before (after) the peak of the laser pulse. This narrow time window is a feature of the tunnel ionization regime, which is characterized by a strong exponential dependence in ionization probability on the laser field strength. The striking accummulation of electrons near $k_z = \pm 2$ a.u., combined with the knowledge that these electrons come from a narrow time window, given by the low-γ tunnel ionization regime, suggests a new method for producing tightly focused electron beams of sub-femtosecond duration.

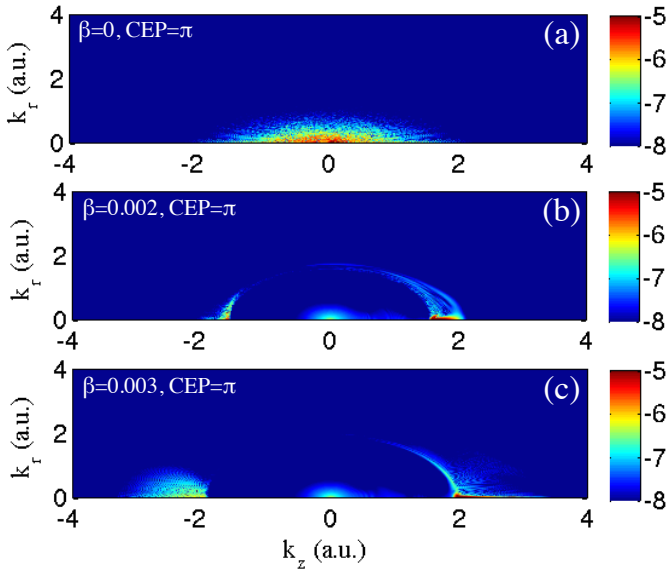

FIG. 4. Two-dimensional electron momentum distributions (k_z, k_r) using the exact 3D TDSE calculation for hydrogen at the laser parameters given in Fig. 1 for three different inhomogeneity parameters β, where $\beta = 0$ corresponds to an homogeneous field.

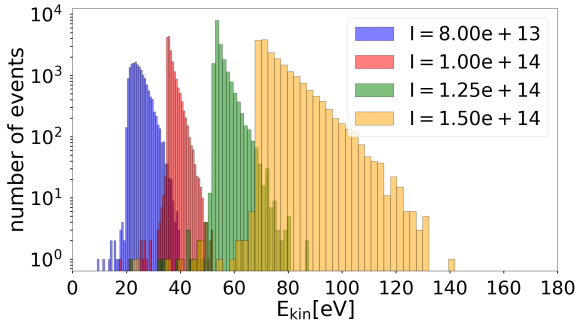

FIG. 5. CTMC simulations of the HES for different laser intensities, for a fixed spatial inhomogeneity: $\beta = 0.002$.

To further investigate the HES as a function of experimental parameters, we performed CTMC simulations for four different CEP phases, corresponding to CEP $= (0, \pi/2, \pi, 3\pi/2)$, at a fixed laser intensity. We also varied the field intensity in the range of $0.8 - 1.5 \times 10^{14} W/cm^2$, corresponding to $E_0 = 0.048 - 0.0654$ a.u. We find that the higher energy structure occurs at all values of CEP, except for $CEP = 0$. In all cases, the electrons forming the higher energy peak come primarily from within a single laser half-cycle, which ionizes in the direction of increasing field. Increasing the laser intensity broadens the peak and shifts it to higher energies, as shown in Fig. 5.

In conclusion, we find a prominent higher energy peak in an "intermediate" regime where the spatial decay length, l_F, of the electric fields is comparable to the electron quiver amplitude. The sensitive $(1/l_F)^2$ dependence of the location and width of the HES on the field decay length suggests a new precise tool for near-field characterization. Finally, the fact that the prominent higher energy peak comes from a narrow time window, well within a single half-cycle of the laser pulse, may be used to create localized sources of monoenergetic electron beams of sub-femtosecond duration. Such sources would take the techniques of classical electron diffraction into the attosecond domain, enabling the investigation of dynamic changes of electron distribution in complex systems, such as nanostructures and biological molecules [67, 68].

J. A. P.-H. and L. R. acknowledge support from Spanish Ministerio de Economa y Competitividad through the FURIAM Project No. FIS2013-47741-R, PALMA project FIS2016-81056-R and LaserLab IV Grant Agreement N 654148. A.S.L. is supported by the Max Planck Center for Attosecond Science (MPC-AS). M. C. was supported by the project ELI-Extreme Light Infrastructure-phase 2 (CZ.02.1.01/0.0/0.0/15 008/0000162) from European Regional Development Fund. A. C. and M. L. acknowledge support from ERC AdG OSYRIS, Spanish MINECO (FIS2013-46768-P FOQUS and Severo Ochoa SEV-2015-0522), Catalan Agaur SGR 874 and Fundaci Cellex. M. F. K. is grateful for support by the EU via the ERC grant ATTOCO (no. 307203) and by the DFG via the excellence center "Munich Centre for Advanced Photonics".

* The first two authors contributed equally; ortmann@pks.mpg.de
† japerez@clpu.es
‡ landsman@pks.mpg.de

[1] R. Pazourek, S. Nagele, and J. Burgdoerfer, Rev. Mod. Phys. **87**, 765 (2015).
[2] A.S. Landsman and U. Keller, Physics Reports, **547** (2015).
[3] P. Agostini, F. Fabre, G. Mainfray, G. Petite, and N. K. Rahman, Phys. Rev. Lett. **42**, 1127 (1979).
[4] F. Grasbon, G. G. Paulus, H. Walther, P. Villoresi, G. Sansone, S. Stagira, M. Nisoli, and S. De Silvestri, Phys. Rev. Lett. **91**, 173003 (2003).
[5] L.V. Keldysh, J. Exp. Theor. Phys. **20**, 1307 (1965).
[6] P.B. Corkum, Phys. Rev. Lett. **71**, (1993).
[7] M. Ferray, A. L'Hullier, X.F. Li, L.A. Lompre, G. Mainfray, C. Manus, J. Phys. B: At. Mol. Opt. Phys, **21** (1988).
[8] F. Krausz and M. Ivanov, Rev. Mod. Phys. **81**, 163 (2009).
[9] M. Lewenstein, *et al.*, Phys. Rev. A **49**, 2117 (1994).
[10] Y. Huismans et al, Science **331**, 61 (2011).
[11] X.B. Bian and A.D. Bandrauk, Phys. Rev. Lett. **108**, 263003 (2012).
[12] J. Itatani, J. Levesque, D. Zeidler, H. Niikura, H. Pepin, J.C. Keiffer, P.B. Corkum, and D.M. Villeneuve, Nature **432**, 867 (2004).

[13] M. Meckel, D. Comtois, D. Zeidler, A. Staudte, D. Pavicic, H.C. Bandulet, H. Pepin, J.C. Kieffer, R. Doerner, D.M. Villeneuve, P.B. Corkum, Science **320**, 1478 (2008).

[14] C.I. Blaga, J.L. Xu, A.D. DiChiara, E. Sistrunk, K. Zhang, P. Agostini, T.A. Miller, L.F. DiMauro, and C.D. Lin, Nature **483**, 194 (2012).

[15] M.G. Pullen, B. Wolter, A.T. Le, M. Baudisch, M. Hemmer, A. Senftleben, C.D. Schroeter, J. Ullrich, R. Moshammer, C.D. Lin, J. Biegert, Nature Commun. **6** 7262 (2015).

[16] C. I. Blaga, F. Catoire, P. Colosimo, G. G. Paulus, H. G. Muller, P. Agostini, and L. F. DiMauro, Nat. Phys. **5**, 335 (2009).

[17] I. Pupeza et al, Nature Photon. **9**, 721 (2015).

[18] J. Dura, N. Camus, A. Thai, A. Britz, M. Hemmer, M. Baudisch, A. Senftleben, C. D. Schr, J. Ullrich, R. Moshammer and J. Biegert, Sci. Rep. **3**, 2675 (2013).

[19] B. Wolter, *et al.*, Phys. Rev. X **5**, 021034 (2015).

[20] F.H. Faisal, J. Phys. B **6**, L89 (1973).

[21] H.R. Reiss, Phys. Rev. A **22** 1786 (1980).

[22] A.D. Bandrauk and S. Chelkowski, Phys. Rev. Lett. **84**, 3562 (2000).

[23] A.S. Landsman, C. Hofmann, A.N. Pfeiffer, C. Cirelli, and U. Keller, Phys. Rev. Lett. **111**, 263001 (2013).

[24] T. Brabec, M.Y. Ivanov, and P.B. Corkum, Phys. Rev. A **54** R2551 (1996).

[25] W. Quan, *et al.*, Phys. Rev. Lett. **103**, 093001 (2009).

[26] C.Y. Wu, Y.D. Yang, Y.Q. Liu, and Q.H. Gong, *et al.* , Phys. Rev. Lett. **109** 043001 (2012).

[27] B. Wolter, C. Lemell, M. Baudisch, M. G. Pullen, X.-M. Tong , M. Hemmer, A. Senftleben, C. D. Schr, J. Ullrich, R. Moshammer, J. Biegert, and J. Burgdorfer, Phys. Rev. A 90 063424 (2014).

[28] M. Möller, F. Meyer, A. M. Sayler, G. G. Paulus, M. F. Kling, B. E. Schmidt, W. Becker, and D. B. Milošević, Phys. Rev. A **90**, 023412 (2014).

[29] C. Liu and K.Z. Hatsagortsyan, Phys. Rev. Lett. **105**, 113003 (2010).

[30] T.M. Yan, S.V. Popruzhenko, M.J.J. Vrakking and D. Bauer, Phys. Rev. Lett. **105**, 253002 (2010).

[31] Q.Z. Xia, D.F. Ye, L.B. Fu, X.Y. Han and J. Liu, Scientific Reports **5** 11473 (2015).

[32] A. Kästner, U. Saalmann, and J.M. Rost, Phys. Rev. Lett. **108**, 033201 (2012).

[33] M. Krueger, M. Schenk, and P. Hommelhoff, Nature **475**, 78 (2011).

[34] F. Süßmann and M. F. Kling, Phys. Rev. B **84**, 121406(R) (2011).

[35] P. Hommelhoff, Y. Sortais, A. Aghajani-Talesh, and M.A. Kasevich, Phys. Rev. Lett. **96**, 077401 (2006).

[36] M. Schenk, M. Krueger, and P. Hommelhoff, Phys. Rev. Lett. **105**, 257601 (2010).

[37] H. Yanagisawa *et al.*, Scientific Reports **6**, 35877 (2016)

[38] S. Choi, et al, Phys. Rev. A **93**, 021405, (2016).

[39] M. Krüger *et al.*, J. Phys. B **45**, 074006 (2012).

[40] G. Herink, D.R. Solli, M. Gulde, and C. Ropers *et al.*, Nature **483**, 190 (2012).

[41] S. Zherebtsov *et al.*, Nat. Phys. **7**, 656 (2011).

[42] F. Süßmann, L. Seiffert, S. Zherebtsov, V. Mondes, J. Stierle, M. Arbeiter, and J. Plenge *et al.*, Nature Commun. **6** 7944 (2015).

[43] B. Förg, J. Schoetz, F. Suessmann, and M. Foerster *et al.*, Nature Commun. **7** 11717 (2016).

[44] S. Kim et al, Nature **453**, 757 (2008).

[45] M. Sivis, M. Duwe, B. Abel and C. Ropers, Nature Physics, **9**, 304 (2013).

[46] M. F. Ciappina et al, Reports on Progress in Physics **80**, 054401 (2017)

[47] M. F. Ciappina, J. A. Pérez-Hernández, T. Shaaran, J. Biegert, R. Quidant, and M. Lewenstein, Phys. Rev. A **86**, 023413 (2012).

[48] T. Shaaran, M. F. Ciappina, and M. Lewenstein, Phys. Rev. A **86**, 023408 (2012).

[49] M. F. Ciappina, J. A. Pérez-Hernández, T. Shaaran, L. Roso, and M. Lewenstein, Phys. Rev. A **87**, 063833 (2013).

[50] G. G. Paulus, *et al.*, Phys. Rev. Lett. **72**, 2851 (1994).

[51] A. Husakou, *et al.*, Phys. Rev. A **83**, 043839 (2011).

[52] X. M. Tong and C. D. Lin, J. Phys. B: At. Mol. Opt. Phys. **38**, 2593 (2005).

[53] L. Ortmann and A.S. Landsman, to be submitted

[54] M.V. Ammosov, N.B. Delone, V.P. Krainov, Sov. Phys.-JETP **64**, 1191 (1986).

[55] N. B. Delone and V. P. Krainov, JOSA B **49** 6 (1991).

[56] Arissian, et al, Phys. Rev. Lett. **105**, 133002 (2010).

[57] A.S. Landsman, A.N. Pfeiffer, C. Hofmann, M. Smolarski, C. Cirelli, and U. Keller, New Journal of Physics **15**, 013001 (2013).

[58] A.S. Landsman and U. Keller, Journal of Physics B: Atomic, Molecular and Optical Physics **47** 204024 (2014).

[59] T. Nubbemeyer, K. Gorling, A. Saenz, U. Eichmann, and W. Sandner, Phys. Rev. Lett. **101** 233001 (2008).

[60] C. Hofmann, A. S. Landsman, C. Cirelli, A. N. Pfeiffer, and U. Keller, Journal of Physics B: Atomic, Molecular and Optical Physics **46** 125601 (2013).

[61] A. N. Pfeiffer, C. Cirelli , M. Smolarski, D. Dimitrovski, M. Abu-samha, L. B. Madsen, and U. Keller, Nature Phys. **8** 76-80 (2012).

[62] T. Zimmermann, S. Mishra, B.R. Doran, D.F. Gordon, and A.S. Landsman, Phys. Rev. Lett. **116**, 233603, (2016)

[63] C. Hofmann, A.S. Landsman, A. Zielinski, C. Cirelli, T. Zimmermann, A. Scrinzi, and U. Keller, Phys. Rev. A **90**, 043406 (2014).

[64] C. Hofmann, T. Zimmermann, A. Zielinski, and A.S. Landsman, New Journal of Physics **18**, 043011 (2016).

[65] A.S. Landsman, S.A. Cohen, and A.H. Glasser, Phys. Rev. Lett. **96**, 015002, (2006)

[66] I. Yavuz, E.A. Bleda, Z. Altun, and T. Topcu, Phys. Rev. A **85**, 013416 (2012).

[67] E. Fill, L. Veisz, A. Apolonski, and F. Krausz, New Journal of Physics **8**, 272 (2006).

[68] C. Kealhofer, W. Schneider, D. Ehberger, A. Ryabov, F. Krausz, P. Baum, Science **352**, 6284 (2016).